Magnetite Nanoparticles (MNPs) Used as Cadmium Metal Removal from the Aqueous Solution from Mill Scales Waste Sources

(Penggunaan Nanozarah Magnetit (MNPs) sebagai Penyingkiran Logam Kadmium daripada Larutan Akua daripada Sumber Sisa Sisik Besi)

Nur Asyikin Ahmad Nazri, Raba'ah Syahidah Azis*, Muhammad Syazwan Mustaffa, Abdul Halim Shaari, Ismayadi Ismail, Hasfalina Che Man, Norlaily Mohd Saiden & Nor Hapishah Abdullah

ABSTRACT

This research carrying out in producing a high percentage of magnetite nanoparticle (MNP) from the waste of industrial mill scales for Cadmium ions removal. The extraction of the magnetite from mill scales waste involved two steps separation technique process known as the Magnetic Separation Technique (MST) followed by Curie Temperature Separation Technique (CTST). The extraction samples were milled using the high energy ball mill (HEBM) at various milling time of 4, 8, 12, 16, and 20 h. The formation of nanosized single-phase hexagonal spinel has been observed as early in 4 h milling time by using XRD analysis. Prolonged the milling time had derived different characteristics of the MNP. The samples then used as an adsorbent in cadmium removal of the aqueous solution. The highest adsorption capacity, qe was contributed by MNP with an 8 h milling time. This is due to the surface area and the porosity of the samples based on BET reports and HR TEM images. Newly extracted MNP from waste mill scales is cost effective and eco-friendly process that potential in wastewater treatment.

Keywords: Adsorbent; adsorption; Cadmium (Cd); heavy metals; magnetite (Fe_3O_4) nanoparticles; waste mill scale; wastewater treatment

ABSTRAK

Penyelidikan ini dijalankan dalam usaha menghasilkan peratusan nanozarah magnetit (MNP) yang tinggi daripada sumber sisa sisik besi untuk penyingkiran ion Kadmium. Pengekstrakan magnetit daripada sisa sisik besi melibatkan proses teknik pemisahan dua langkah yang dikenali sebagai Teknik Pemisahan Magnetik (MST) diikuti oleh Teknik Pemisahan Suhu Curie (CTST). Sampel pengekstrakan dikisar menggunakan pengisar bola tenaga tinggi (HEBM) pada pelbagai waktu pengisaran 4, 8, 12, 16 dan 20 jam. Pembentukan spinel heksagon fasa tunggal saiz nano telah diperhatikan seawal masa pengisaran 4 jam dengan menggunakan analisis XRD. Masa pengisaran yang berpanjangan telah menghasilkan ciri MNP yang berbeza. Sampel kemudian digunakan sebagai penyerap dalam penyingkiran kadmium dalam larutan akua. Kapasiti penjerapan tertinggi, qe disumbangkan oleh MNP dengan masa pengisaran 8 jam. Ini disebabkan oleh luas permukaan dan keliangan sampel berdasarkan laporan BET dan imej HR TEM. MNP yang baru diekstrak daripada sisa sisik besi adalah proses yang menjimatkan dan mesra alam yang berpotensi dalam rawatan air sisa.

Kata kunci: Kadmium (Cd); logam berat; nanozarah magnetit (Fe_3O_4); penjerap; penjerapan; sisa sisik besi; rawatan air sisa

Introduction

Over the past few decades, heavy metal pollution has become a serious environmental problem. Heavy metal refers to any metallic chemical element that has a relatively high density and is toxic or poisonous at low concentrations. Examples of heavy metals include: cobalt (Co), copper (Cu), chromium (Cr), iron (Fe), magnesium (Mg), manganese (Mn), molybdenum (Mo), nickel (Ni), selenium (Se), zinc (Zn), arsenic (As), mercury (Hg), lead (Pb), and cadmium (Cd). Cadmium derives its toxicological properties from its chemical similarity to zinc, an essential micronutrient for plants, animals, and humans. Cadmium is bio-persistent and, once absorbed by an organism, remains residents for many years (over decades for humans) even it is eventually excreted. In humans, long-term exposure is associated with renal dysfunction. High exposure can lead to obstructive lung disease and has been linked to lung cancer despite data concern the latter is difficult to interpret due to compound factors. Cadmium may also produce bone defects (osteomalacia, osteoporosis) in humans, and animals. In addition, the metal can be linked to increase blood pressure

and effects on the myocardium in animals, even with most human data do not support these findings. A major source of Cd pollution comes from the industrial wastewater stream such as effluents from electroplating, battery, metal finishing, and printed circuit board industries. Due to the importance of removing Cd from the wastewater, several methods have been developed to treat the waste water contains heavy metal pollution.

Adsorption is an effective, simple and economic process that removes heavy metal ions by contacting adsorbents with wastewater by applying an external magnetic field (Ghasemie et al. 2017; Li et al. 2017; Mohan & Pittman 2007; Monier et al. 2010; Sodipo & Aziz 2016). The most studied magnetic adsorbent was magnetite (fe3o4). This is due to the good potential for having a higher magnetic response with higher saturation magnetization at the lower size. Nano-sized Fe3O4 particles have a large surface areas that increases more metal ions attraction in wastewater applications. Besides, a large production of the magnetite is one of the conditions to be used as a good adsorbent (Kumar et al. 2015; Rajput et al. 2016; Sodipo & Aziz 2016). Taking both economic and environmental problems into account and the high consumption of chemicals in the production of fe3o4 nanoparticles, an alternative way was proposed as a new approach that is to derive or extract fe3o4 from the mill scales waste and applying them in wastewater treatment.

Mill scales waste is a waste material that produces from the hot rolling of steel in many steel factories. Mill scales waste is rich irons contain (about 99% iron) and a small amount of impurities (1% of other compounds; such as C, Si, & Mn) (Azis et al. 2018, 2002a, 2002b; Daud et al. 2015). In a steel making production of steel factories, it is common during the hot rolling steel, the iron oxides were formed into the surface of the steel, and called as scales. The abundance of scales is defined as mill scales. The iron oxides of the mill scales waste are consisting of iron oxide elements, such as wustite (FeO), magnetite (Fe_3O_4), hematite (Fe_2O_3) along with small amount impurities, such as carbon, barite and steel powders, metal shavings, and steel punchings (Azis et al. 2018, 2002a, 2002b; Daud et al. 2015).

Thus, this research works on the synthesis of magnetite by using separation technique followed by HEBM (4, 8, 12, 16, and 20 h) has been employed in order to observe the effect of varied particle sizes of the Cd (II) adsorption.

METHODS

SAMPLES PREPARATION (ADSORBENT)

The Raw waste industrial mill scales were collected from steel factories located in Malaysia. Impurities such as stone, sands, dust or pieces of plastic were removed in order to avoid contamination in the samples. The mill scales were crushed using conventional steel ball milling

for 72 h. The milled powder was purified by using the separation I: Magnetic Separation Technique (MST), to separate the magnetic and non-magnetic powder. The magnetic powder then preceded using separation II: Curie Temperature Separation Technique (CTST), to extract stronger magnetic materials. The waste mill scales separation routes (separation I and II) were done similar to previous report by Azis et al. (2018), (2002a), (2002b), and Daud et al. (2015). The magnetite (Fe3O4) yields to CTST was dried in the oven at 120 oC for 24 h. The magnetite powder was milled using the SPEX 8000D milling machine with the ball to powder (BPR) ratios of 10:1 for 4, 8, 12, 16, and 20 h.

Adsorbate

All compounds that were used to prepare reagent solutions were analytical reagent grade. The stock solution of Cadmium nitrate (Cd(NO3)2) (Sigma-Aldrich, UK) (1000 µgL^{-1}) is prepared by dissolving a weighed quantity of the respective Cadmium nitrate in deionized water. The concentration of the metal solution and pH used in this work was 500 µgL^{-1} with pH 5. Then, 50 mg of fe3o4 nanoparticles adsorbent was added to the 50 mL of Cd solution and placed in the vibrator bath (Variable speed reciprocal vibrator (model HY-8) with fixed 160 rpm for 20 min. All the adsorption tests were carried out at room temperature 22-25 C in a shaker by mixing accurately the weighed amounts of adsorbents with adsorbate solutions to specific concentrations in a covered bottle. pH 5 value was maintained for the solution.

SAMPLES CHARACTERIZATION

Structural and phase composition

The structural and phase composition of samples were collected with X-ray diffraction (Philips Expert PW3040 diffractometer) operating in 40 kV and 40 mA with CuKα radiation (λ = 0.154 nm).

Particle size and morphology

The morphology, particle size, and atom arrangement of the samples were observed using a JEM JEOL 2100 HR transmission electron microscope.

IR spectroscopic analysis

Infrared spectra (200-4000 cm^{-1}) were recorded using FTIR spectrometer (Thermo Nicolet, Model Nicolet 6700).

Magnetic properties

The magnetic properties of samples were measured by a vibrating sample magnetometer (VSM) LAKESHORE

Model 7404. The measurement was carried out at room temperature. The external field of 0- 13 kOe (kG) was applied parallel to the sample.

Surface area measurement

The BELSORP-mini II Brunauer–Emmett–Teller (BET) machine was used to measure the specific surface area and pore size of the samples. The N2 absorption desorption at the liquid nitrogen (N2) temperature using a NOVA2200e automatic surface area and porosity analyzer. In about 0.2 mg of samples was degassed at 120oC for 8 h under 1 Pa vacuum condition before measurement to remove the humidity in the samples. Nitrogen gas was purged with 10-100 mL/min of the gas flow into the sample cell and, the samples were put into a Dewar vessel containing 2 L of nitrogen liquid. The measurement of the surface area per mass was determined.

Adsorption

In this experiment initial concentration used was 500 μg/L. The pH of the solution was measured using the pH meter. The adsorption capacities of the Cd (II) concentration on the solutions was determined using atomic absorption spectrometer (AAS) (Thermo Scientific iCE 3000 Series Solaar AA). The initial and final concentrations of the sample solutions were measured by AAS. The percentage metal removal (%) was calculated using (1):

$$Removal\,(\%) = \frac{c_i - c_f}{c_i} \times 100\%$$

where C_i is the initial concentration; and C_f is the concentration after treatment with nanoparticles.

RESULTS AND DISCUSSION

STRUCTURAL AND MICROSTRUCTURAL ANALYSIS

Figure 1(a) shows the XRD spectra of the particles of raw mill scale, after undergoing MST and CTST. Figure 1(b) shows the XRD pattern subjected to samples after HEBM for 4, 8, 12, 16, and 20 h, respectively. The XRD pattern given by the raw mill scales shows that the peaks matched with magnetite and hematite (Tables 1 & 2, Figure 1). For hematite (Fe2O3), the peaks can clearly be seen at 104 (33.33), 116 (54.36) and 1010 (72.40). After the first separation (MST), there are new peaks contributed by the presence of wustite (FeO) at 111 (36.33), 002 (42.19), and 022 (61.20). After the second separation, the XRD spectra show an additional peak of wustite at 003 (36.39) and 110 (61.33). The effect of high energy ball milling from 4 h to 20 h towards the sample could be observed in Figure 1(b). As shown, diffraction peaks of all samples after HEBM completely correspond to standard pattern characteristic peaks of the magnetite hexagonal inverse spinel structure (JCPDS: 98-005-9302) 110 (30.1), 113 (35.45), 024 (43.07), 125 (56.97), 208 (62.47). As can be seen from the spectra, the main peaks which correspond to hkl (113) were observed to be broader as the milling time increased. This is due to particle size decrement and the increase in lattice strain. The collision occurred during high energy ball milling that has induced stress inside the powder particles. There are three stages that occurs to high energy ball milling, at the first staged, fracturing dominates the welding process. Most energy impacted on the particles is used to work hardened and fracture the particles. At the second stage, fracturing and cold welding still ongoing but in reverse where fracturing dominated over. The cold welding refined the structure but maintain the average particle size of the powders (Suryanarayana 2001).

TABLE 1. The peak position (2θ), FWHM (2θ), hkl, d-spacing, height (counts), ICSD reference code, composition and chemical formula of raw waste mill scales, MST, and CTST

Milling time	Pos. (2θ)	FWHM (2θ)	*hkl*	*d*-spacing	Height (cts.)	ICSD	Comp.	Chem. formula	Crystal structure	Space group
RMS	35.66	0.1000	113	2.5158	10011.98	98-010-9827	Magnetite (79%)	Fe_3O_4	Cubic	F d -3 m
	33.32	0.1000	104	2.6858	1676.37	98-004-6404	Hematite (21%)	Fe_2O_3	Hexagonal	R -3 c
MST	35.70	0.1000	113	2.5124	9855.48	98-001-7127	Magnetite (0.1%)	Fe_3O_4	Orthorhombic	I m m a
	42.27	0.1000	012	2.1360	110.67	98-000-6336	Wuestite (99.9%)	$Fe_{0.856}O$	Hexagonal	A b m 2
CTST	35.70	0.3722	113	2.5124	9855.48	98-010-9828	Magnetite (59%)	Fe_3O_4	Cubic	F d -3 m
	42.27	0.1000	012	2.1360	110.37	98-001-2336	Wuestite (41%)	$Fe_{0.942}O$	Hexagonal	R -3 m

TABLE 2. The peak position (2), FWHM (2), hkl, d-spacing, height (counts), ICSD reference code, composition, and chemical formula for HEBM powder at various milling

| Milling time	Pos. (20)	FWHM (20)	*hkl*	*d*-spacing	Height (cts.)	ICSD	Comp.	Chem. formula	Crystal structure	Space group
4	35.48	0.1000	113	2.5279	4215.03	98-005-9302	Magnetite (100%)	Fe_3O_4	Hexagonal	R -3 m
8	35.45	0.1000	113	2.5300	488843.47	98-005-9302	Magnetite (100%)	Fe_3O_4	Hexagonal	R -3 m
12	35.45	0.1000	113	2.5300	4843.47	98-005-9302	Magnetite (100%)	Fe_3O_4	Hexagonal	R -3 m
16	35.45	0.1000	113	2.5300	5813.97	98-005-9302	Magnetite (100%)	Fe_3O_4	Hexagonal	R -3 m
20	35.45	0.1000	113	2.5300	4843.47	98-005-9302	Magnetite (100%)	Fe_3O_4	Hexagonal	R -3 m
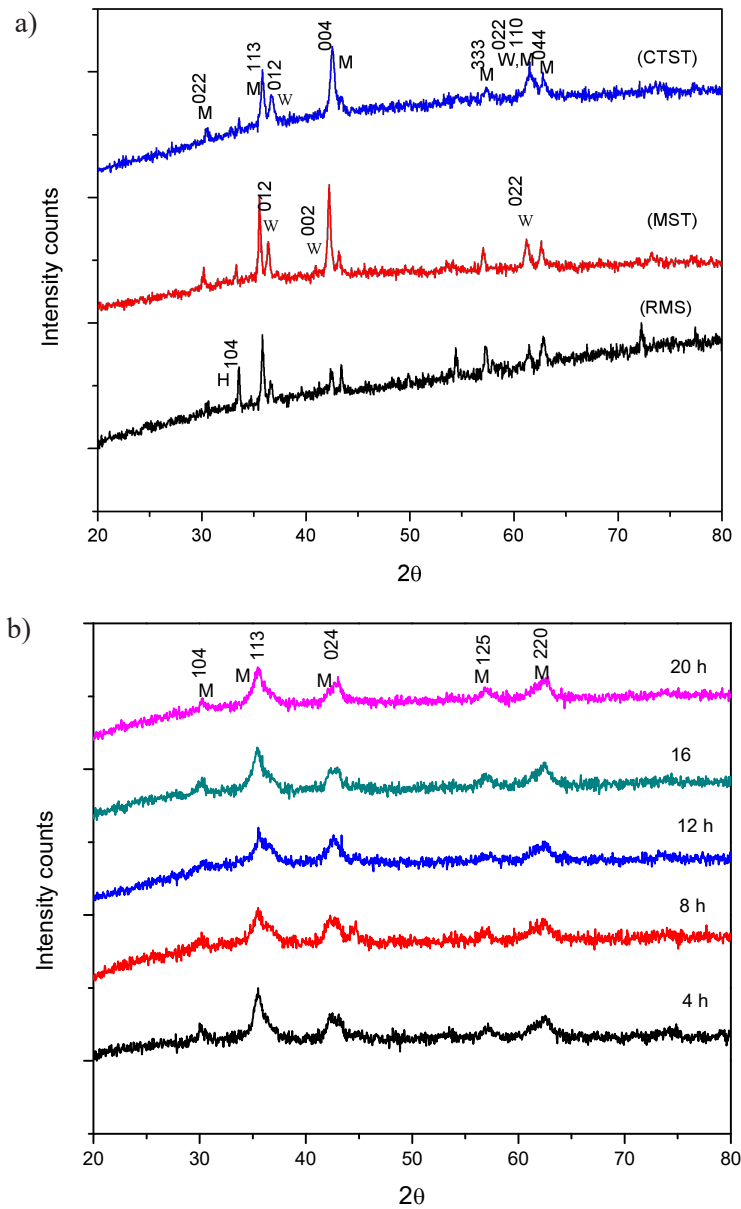
FIGURE 1. XRD patterns for before HEBM (a) RMS, MST, and CTST. XRD patterns for after HEBM (b) 4, 8, 12, 16, and 20 h

Figure 2 shows HRTEM images and the particle size was measured by taking diameters of 200 particles. After MST and CTST separation technique, the particle was in the range of 532 and 356 nm (Figure 2(a) and 2(b)). Larger particle size was observed as convinced of the XRD results in which sharper peaks occurred in the sample. After carrying out the high energy ball milling process of 4 h to 20 h (Figure 2(c)-2(g)), the particle sizes were observed to be decreased, as the milling time increased due to the kinetic energy generated by the series of collisions among balls is transferred to the system (Suryanarayana et al. 1992). The nanoparticles were agglomerated, indicating good connectivity between the grains together. It was occurred due to large surface areas, magnetic forces, and subjected with cold welding and fracturing of the HEBM process. The agglomeration

was reduced with an increase in grain growth. Figure 3 shows an electron beam diffraction pattern recorded from an array structured nanoparticles for sample milling at 8 h. The electron beam diffraction patterns recorded from a large number of nanostructured particles shows a unique pattern, with a sharp beam spot, which represent the lattice planes in the diffraction pattern. Each ring corresponds to atomic planes of different orientation and different inter-planar spacing d. The grains in a specimen are randomly oriented, diffraction spots occur at all angles and give the appearance of continuous rings (Egerton 2005). However, in this work, the value of the grain size having greater than the size presented in the electron diffractometer. This occurs may be due to the agglomeration of the magnetic nanoparticles.

a) MST (532 nm)

200 nm

b) CTST (356 nm)

100 nm

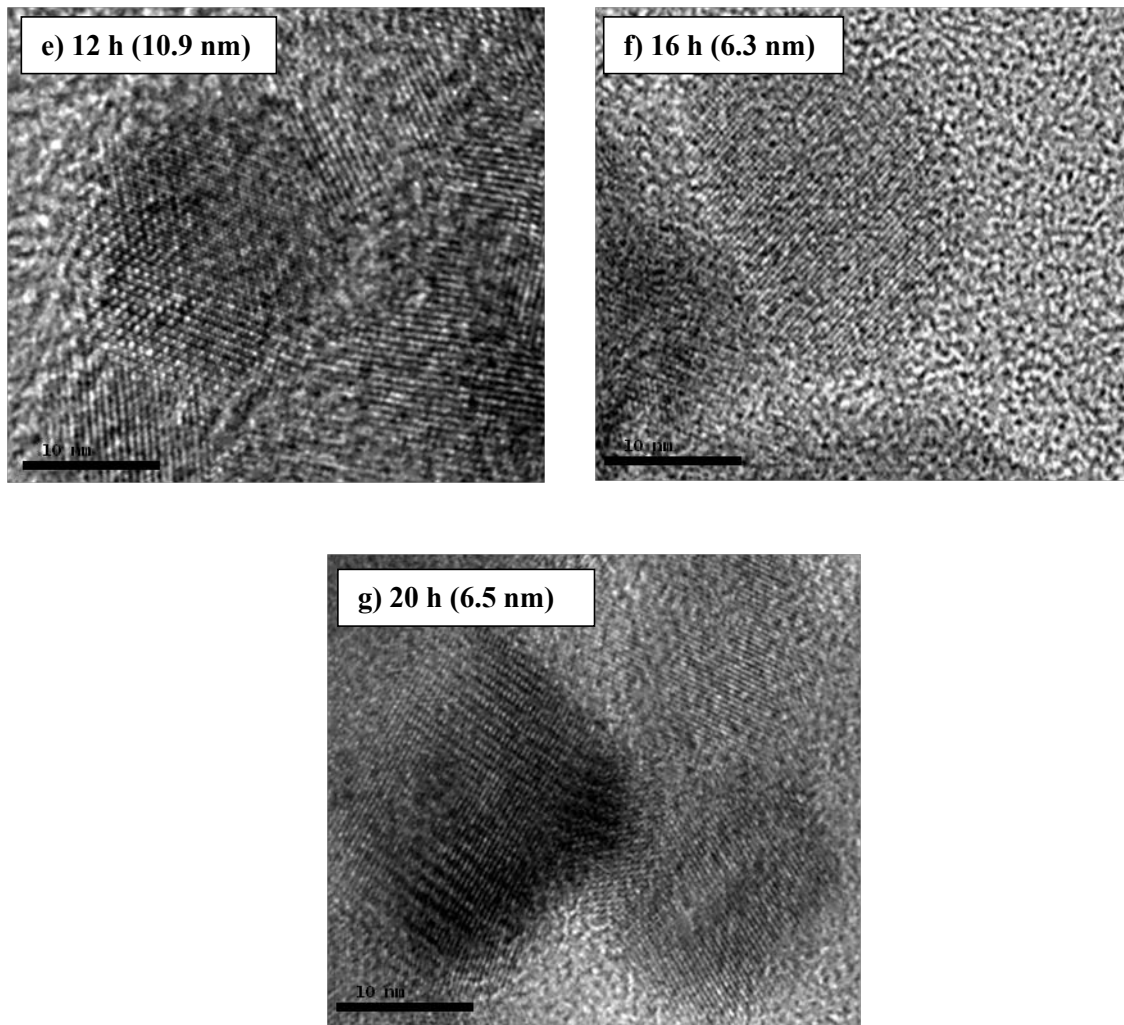c) 4 h (16.2 nm)

10 nm

(d) 8 h (13.1 nm)

10 nm
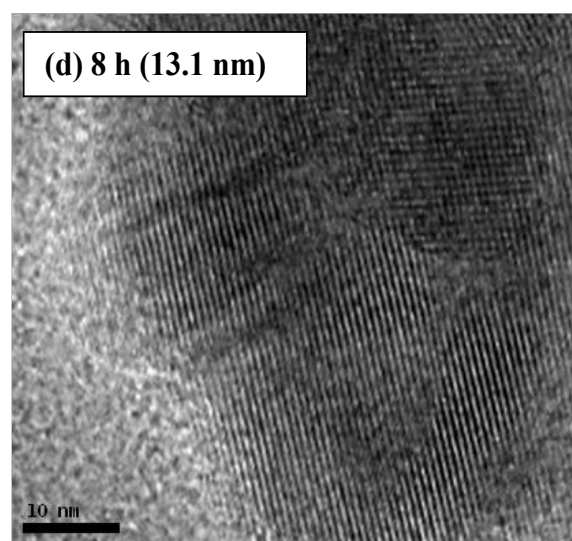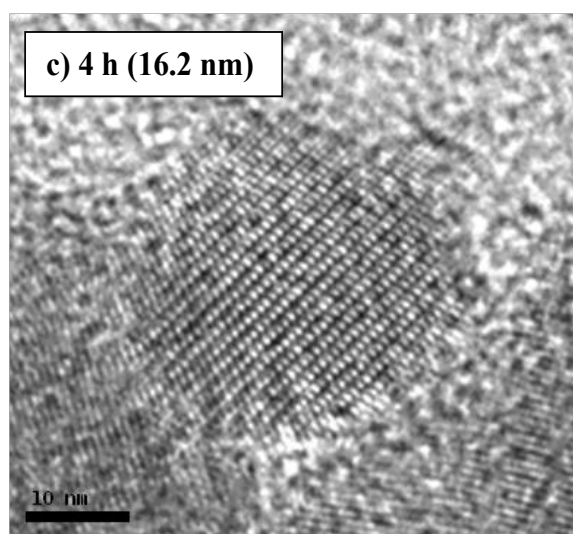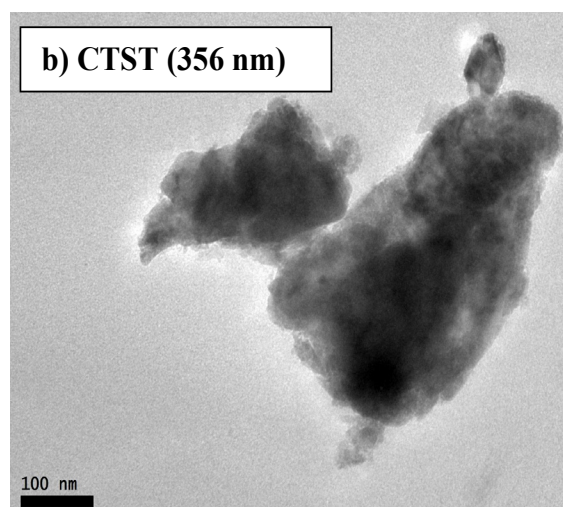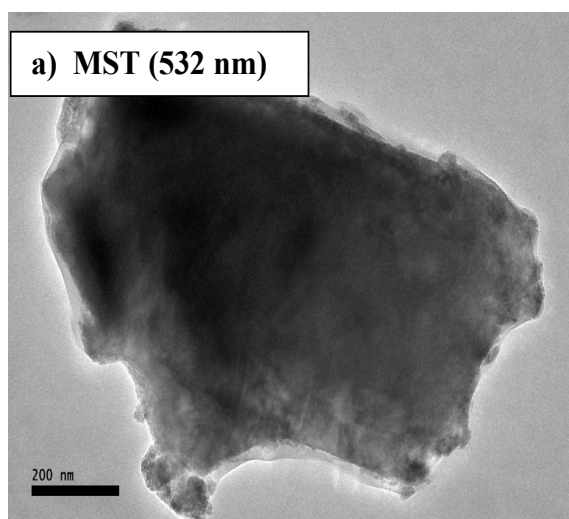
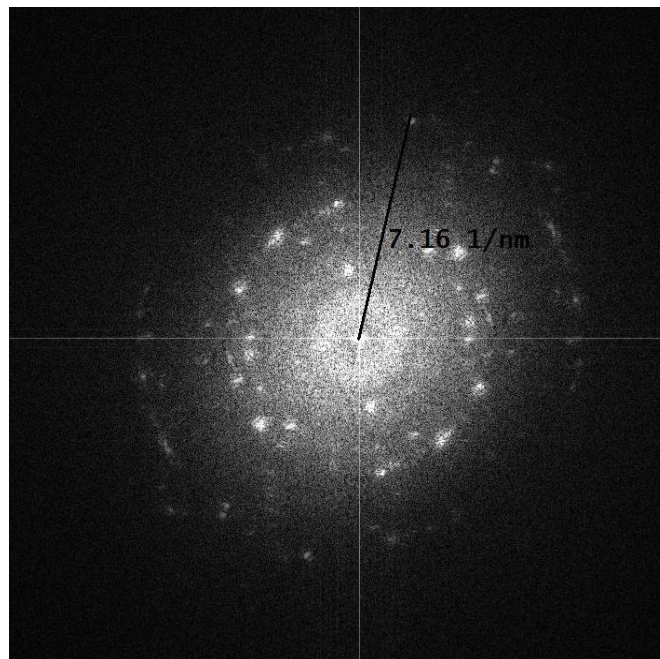FIGURE 2. HRTEM images with particle size for each sample

FIGURE 3. Electron diffraction images for samples 8 h milling time

Figure 4 shows FTIR transmittance spectra of the samples. The spectra for a, b, and c samples presents a band at 590 cm^{-1} (in the magnetite transmission region), whereas spectra for d, e, f, g, and h samples show a broad band between 590 and 650 cm^{-1}, in the magnetite and maghemite transmission region (Andrade et al. 2010; Muda et al. 2016). The FTIR shows the vibration characteristic of transmittance bands that attributed to Fe−O vibrations (Muda et al. 2016). The strongest absorption band of 570 cm^{-1} specifies the presence of Fe-O bands of magnetite nanoparticles (Bruce et al. 2004). These results are in close agreement with the theoretical values and indicate that the sample is Fe_3O_4. The transmittance bands at 582, and 430 cm^{-1} associated with the stretch vibration mode and

torsional vibration mode of Fe-O bonds in the tetrahedral sites and in the octahedral sites. In comparison with the literature, these two IR peaks of the samples are shifted to higher wavenumbers due to the ultrafine particle sizes (Andrade et al. 2010). When, the size of magnetite (Fe_3O_4) particles is reduced to nanoscales dimensions, the bond force constant increases. It is because of large numbers of bonds involving surface atoms are broken, resulting in a rearrangement of non-localized electrons on the particle surface (Schwertmann & Cornell 2008). Therefore, the FTIR spectrum of Fe_3O_4 nanoparticles exhibits a blue shift and the characteristic absorption bands of the Fe-O bond are shifted to high wavenumbers by about 590 cm^{-1}.
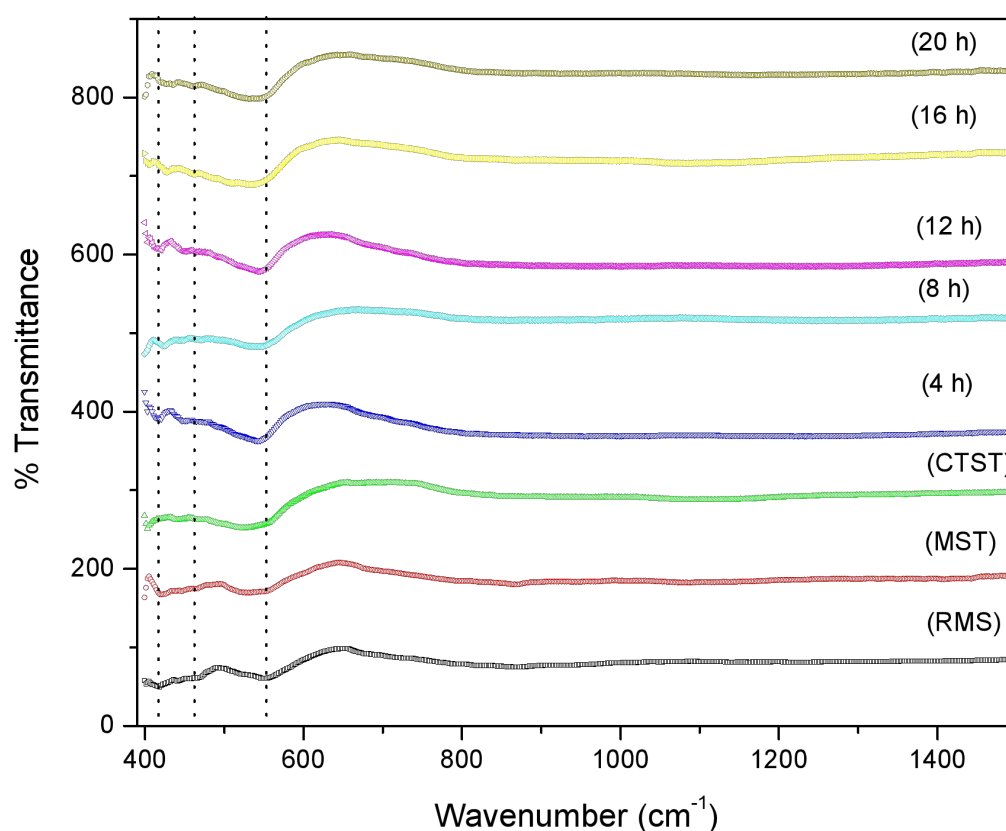

FIGURE 4. FTIR transmittance pattern for RMS, MST, CTST, and milled Fe3O4 at 4, 8, 12, 16, and 20 h

MAGNETIC PROPERTIES ANALYSIS

Figure 5 shows the magnetization of the samples as a function of the applied magnetic field (M-H curves) at room temperature for all prepared samples. The details of the value of saturation magnetization, Ms, and coercivity, Hc for each process have been proposed in Figure 5 and Table 3. Samples that undergo high energy ball milling from 4 h up to 20 h were observed to fall in superparamagnetism group, since the critical size for super-paramagnetic behavior is about 20 nm.

The particles are in a single domain and thermal energy unable to overcome the anisotropy energy barrier for spin reversal. It exhibits typical ferrimagnetic behavior (Hah 2016; Liu et al. 2006; Parkinson 2016). As can be seen in Figure 6, the magnetization value reaches its highest value of 8 h and started to decrease to subsequent milling time. Lower fractions of magnetite phases observed in RM, MST, and CTST lead to a lower value in saturation magnetization. The effect of increasing the milling time furthered than 8 h has resulted

in lower value of the saturation magnetization which might be due to the fracturing and welding process that causes more defects when prolonged milling time (Tan et al. 2015). In addition, magnetic hysteresis loops measured at room temperature. The magnetization values observed in nanostructure materials are smaller than the corresponding bulk materials, assuming that is no changes in ionic configurations occurred. The reduction and lack of saturation after that are likely related to the smaller particle size and high surface areas, which could lead to some spin canting (Blaney 2007). Generally,

the Hc value as depicted in Figure 6 shows that the value was decreased as the samples have undergone stages of milling time due to superparamagnetism behavior that is in the single domain regions. It requires less energy to overcome anisotropy fields inside the samples. The samples sintered at RM and MST stage exhibit multi-domain grains behavior. The transition to the multi-domain to single domains occurred once when the sample started undergone HEBM process of 4 h indicating, respectively, higher superparamagnetic phase crystallinity.
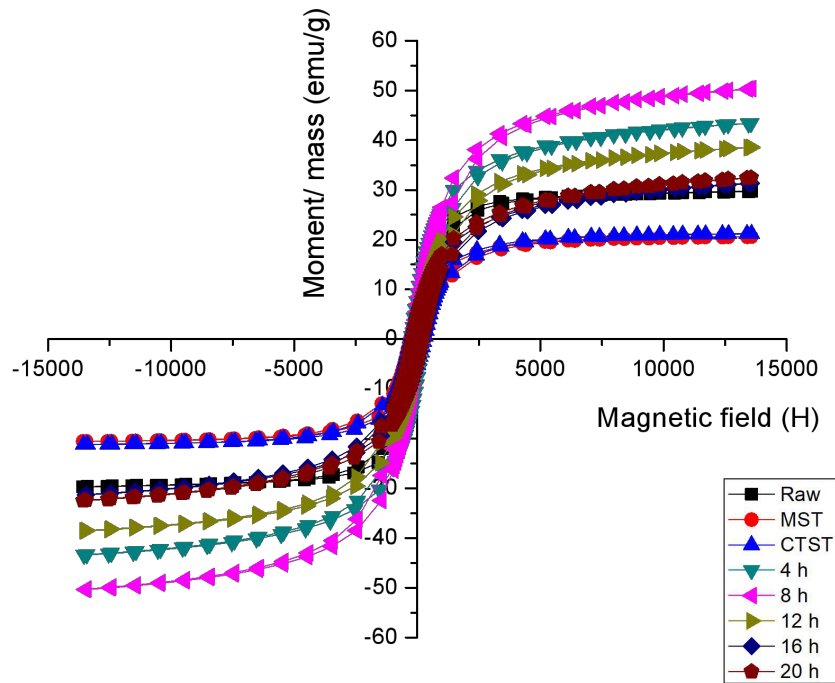

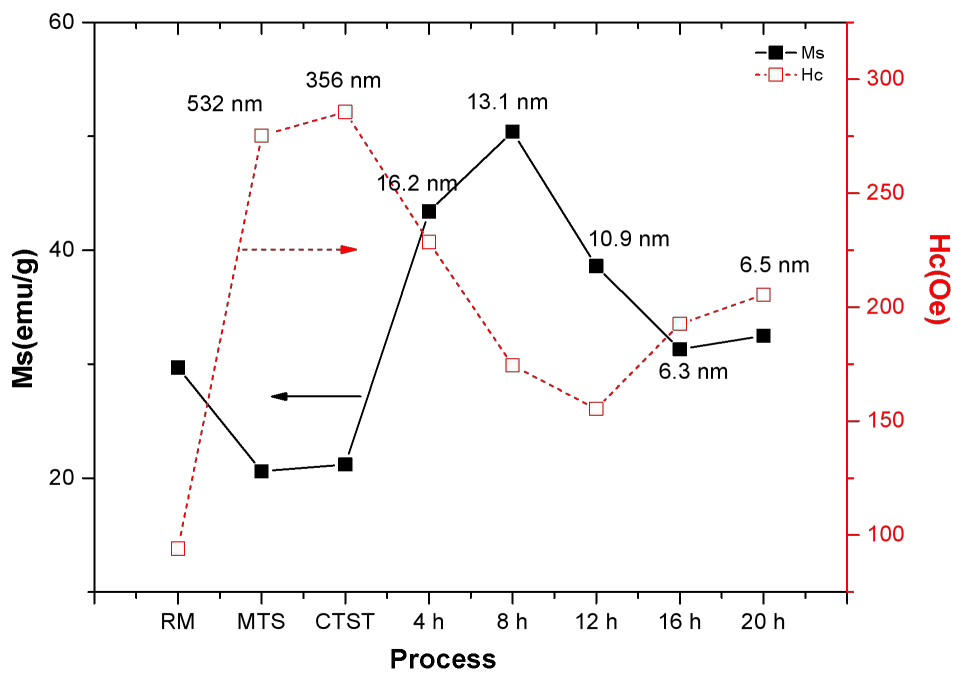FIGURE 5. Magnetic hysteresis loops for each sample

FIGURE 6. Saturation magnetization and coercivity as a function of the process with different particle size

TABLE 2. The peak position (2), FWHM (2), hkl, d-spacing, height (counts), ICSD reference code, composition, and chemical formula for HEBM powder at various milling

Adsorbents	Saturation magnetization M_s (emu/g)	Coercivity H_c (Oe)	*Particle size (nm)*
Raw	29.7	94	> 600
MST	20.6	275.3	532
CTST	21.2	285.7	356
4	43.4	228.6	16.2
8	50.4	174.4	13.1
12	38.6	155.4	10.9
16	31.3	192.7	6.3
20	32.5	205.5	6.5

ADSORPTION PROPERTIES ANALYSIS

Based on Figure 7(a), the raw mill scales with micron size having very low surface areas which is 0.5171 m2/g. Interestingly, it observed adsorption of Cu removal is about 57%. This maybe contributes by the porosity of the mill scale surfaces where the diameter of the porosity measured was 361.798. The same case also for samples after MST and CTST, where showed quiet high removal percentage (Figure 8). This may due to the porosity surfaces as confirmed by FESEM images. Nevertheless, the surface areas of both samples are higher compared to raw mill scales. This also contributes to higher removal of Cd by these two adsorbents. Four and 8 h adsorbents are in nanoscale where the surface area increased with the lower particle size. In addition, the saturation magnetization may also contribute to higher removal of Cd. Prolonged the milling time was cause a drop to the adsorption percentage and the size also the surface area. Therefore, from all the samples, we can say that 8 h showed the best performance in removing Cd. Since this is the first paper that reported on magnetite that synthesized by a raw mill scale on Cd removal, there is no previous work to be compared. Due to the successful adsorption experiment, magnetite from raw mill scales synthesized using mechanical alloying has potential in other applications especially to solve environmental problems (Shahid et al. 2018).
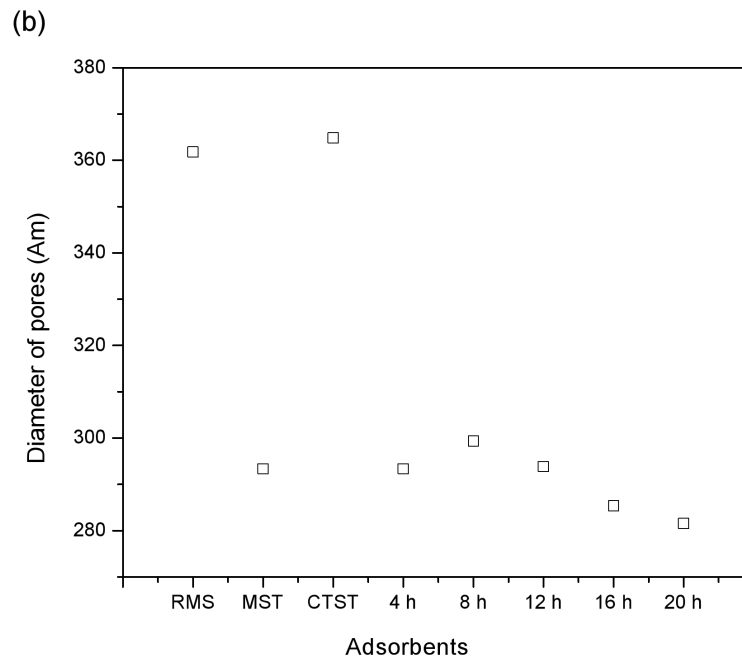
(a)

(b)
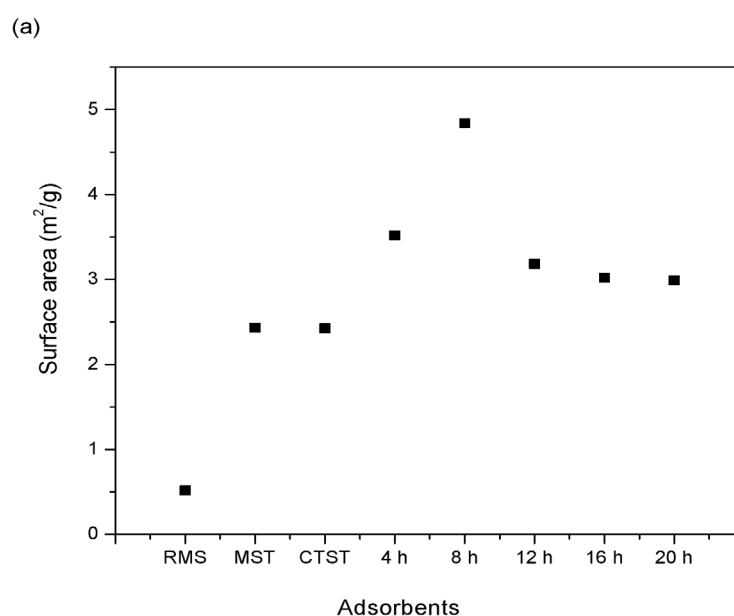
FIGURE 7. (a) Surface area and (b) porosity of diameter as a function of different adsorbents

Figure 8 shows the adsorption capacity, qe as a function of different adsorbents. The amount of adsorbate is taken up by an adsorbent as the function of the concentration of adsorbate at a constant temperature which called as the adsorption capacity. It can be calculated as (2):

$$q_e = \frac{v}{m} \quad (C_o - C_e) \quad \quad (2)$$

where q_e (mg/g) is the amount of adsorbate per unit mass of adsorbent at time t; C_o and C_e were the initial and final concentrations (µg/L) of the solution, respectively. V is the volume of the solution to liters, and m is the mass of the adsorbent in grams (g).

The highest adsorption capacity was shown by magnetite after 8 h with 488.2 µg/g. An optimum milling time for the best adsorption capacity was 8 h. The decrease of adsorption capacity and, the increase in milling time was due to cold welding and fracturing that occurred with prolonging milling time.
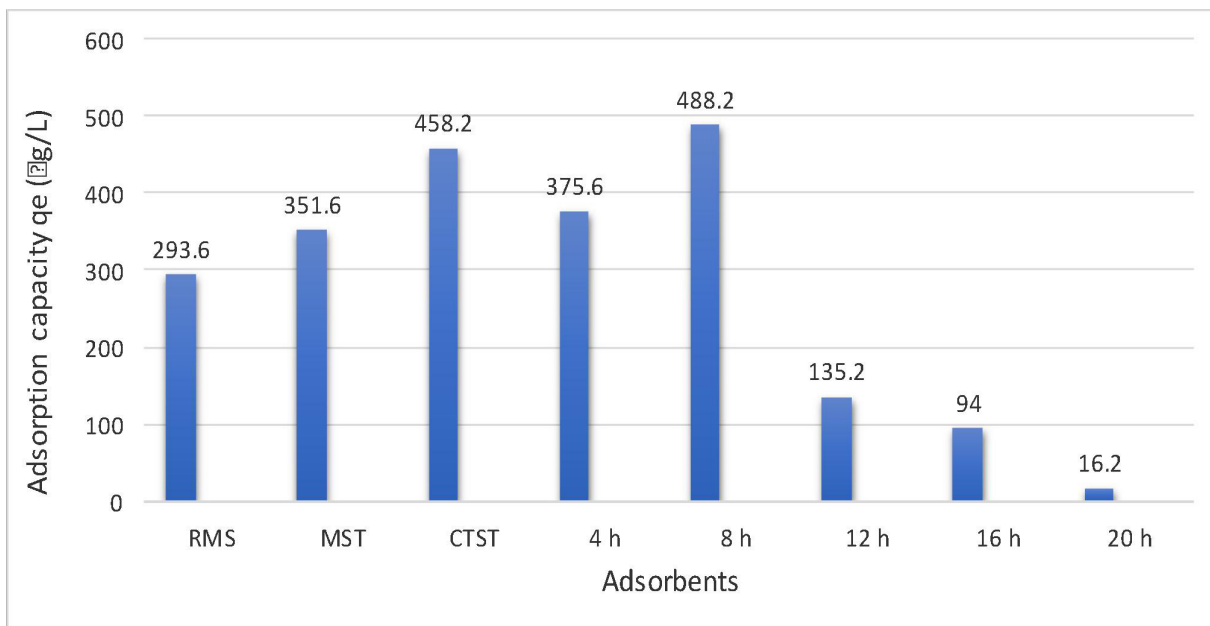

FIGURE 8. Adsorption capacity, q_e as a function of different adsorbents

TABLE 2. The peak position (2), FWHM (2), hkl, d-spacing, height (counts), ICSD reference code, composition, and chemical formula for HEBM powder at various milling

Adsorbents	Cd removal (%)	Surface area (m^2/g)	Porosity	Particle size (nm)
RMS	50	0.5171	361.798	> 600
MST	70	2.432	293.3449	532
CTST	90	2.424	364.8565	356
4	75	3.5197	293.3449	16.2
8	100	4.8407	299.3449	13.1
12	30	3.1817	293.842	10.9
16	20	3.0182	285.365	6.3
20	5	2.991	281.563	6.5

CONCLUSION

This study proved that mill scales waste has good potential to be used in adsorption of Cd ions from aqueous solutions. This work successfully turned mill scales waste into useful magnetite nanoparticles with higher magnetic properties. HEBM technique helps to refine the size of the particles to good distribution percentages other than reducing the size. The adsorption capacity of the best milling time producing magnetite is at 8 h which is 488.2 µg/g. The results from the FTIR showed that there is adsorption occurs to the magnetite when the spectrum shows changes after the adsorption. Further research needs to be done with respect to the utilization of waste mill scales of Cd removal in the wastewater treatment plant such as sorption-desorption cycles for its regeneration and reuse.

REFERENCES

Andrade, Â.L., Souza, D.M., Pereira, M.C., Fabris, J.D. & Domingues, R.Z. 2010. pH effect on the synthesis of magnetite nanoparticles by the chemical reduction-precipitation method. *Quimica Nova* 33(3): 524-527.

Azis, R.S., Syazwan, M.M., Shahrani, N.M.M., Hapishah, A.N., Nazlan, R., Idris, F.M., Ismail, I., Zulkimi, M.M.M., Ibrahim, I.R., Abbas, Z. & Saiden, N.M. 2018. Influence of sintering temperature on the structural, electrical and microwave properties of yttrium iron garnet (YIG). *Journal of Materials Science Materials in Electronics* 29: 8390-8401.

Azis, R.S., Hashim, M., Yahya, N. & Saiden, N.M. 2002a. A study of sintering temperatures variation on microstructure developments of strontium hexaferrite millscale-derived. *Journal of Applied Sciences* 2(12): 1092-1095.

Azis, R.S., Hashim, M. & Yahya, N. 2002b. Purified iron oxide -Fe$_2$O$_3$ from millscale using curie temperature separation technique. *Journal of Solid State Science and Technology* 9: 87-90.

Blaney, L. 2007. Magnetite (Fe$_3$O$_4$): Properties, synthesis, and applications. *Lehigh Review* 15: 33-81.

Bruce, I.J., Taylor, J., Todd, M., Davies, M.J., Borioni, E., Sangregorio, C. & Sen, T. 2004. Synthesis, characterisation and application of silica-magnetite nanocomposites. *Journal of Magnetism and Magnetic Materials* 284: 145-160.

Daud, N., Azis, R.S., Hashim, M., Matori, K.A., Hassan, J., Saiden, N.M. & Shahrani, N.M.M. 2015. Preparation and characterization of Sr1−xNdxFe12O19 derived from steelwaste product via mechanical alloying. *Materials Science Forum* 846: 403-409.

Egerton, R.F. 2005. *Physical Principles of Electron Microscopy.* New York: Springer.

Ghasemi, E., Heydari, A. & Sillanpää, M. 2017. Superparamagnetic Fe$_3$O$_4$@ EDTA nanoparticles as an efficient adsorbent for simultaneous removal of Ag(I), Hg(II), Mn(II), Zn(II), Pb(II) and Cd(II) from water and soil environmental samples. *Microchemical Journal* 131: 51-56.

Hah, H.Y. 2016. Magnetism of magnetite nanoparticles as determined by Mössbauer spectroscopy. Master's Thesis. University of Tennessee (Unpublished).

Kumar, R., Sakthivel, R., Behura, R., Mishra, B.K. & Das, D. 2015. Synthesis of magnetite nanoparticles from mineral waste. *Journal of Alloys and Compounds* 645: 398-404.

Liu, X.Q., Guan, Y.P., Chen, H.H., Liu, H.Z. & Axel, J.R. 2006. Preparation and characterization of hydrophobic superparamagnetic magnetite gel. *Journal of Magnetism and Magnetic Materials* 306: 248-253.

858

Li, J., Jiang, B., Liu, Y., Qiu, C., Hu, J., Qian, G., Guo, W. & Ngo, H.H. 2017. Preparation and adsorption properties of magnetic chitosan composite adsorbent for Cu^{2+} removal. *Journal of Cleaner Production* 158: 51-58.

Mohan, D. & Pittman, Jr. C.U. 2007. Arsenic removal from water/wastewater using adsorbents-A critical review. *Journal of Hazardous Materials* 142(1-2): 1-53.

Monier, M., Ayad, D.M., Wei, Y. & Sarhan, A.A. 2010. Adsorption of Cu(II), Co(II), and Ni(II) ions by modified magnetic chitosan chelating resin. *Journal of Hazardous Materials* 177(1-3): 962-970.

Muda, N.N.C., Azis, R.S., Shaari, A.H., Hassan, J. & Sulaiman, S. 2016. Elemental analysis and IR band characteristics of -Fe_2O_3 and $BaFe_{12}O_{19}$ steel waste product based. *Solid State Science and Technology* 24(2): 45-51.

Parkinson, G.S. 2016. Iron oxide surfaces. *Surface Science Reports* 71(1): 272-365.

Rajput, S., Pittman, Jr. C.U. & Mohan, D. 2016. Magnetic magnetite (Fe_3O_4) nanoparticle synthesis and applications for lead (Pb^{2+}) and chromium (Cr^{6+}) removal from water. *Journal of Colloid and Interface Science* 468: 334-346.

Schwertmann, U. & Cornell, R.M. 2008. *Iron Oxides in the Laboratory: Preparation and Characterization.* 2nd ed. Weinheim, Germany: Wiley-VCH Verlag.

Shahid, M.K., Phearom, S. & Choi, Y.G. 2018. Synthesis of magnetite from raw mill scale and its application for arsenate adsorption from contaminated water. *Chemosphere* 203: 90-95.

Sodipo, B.K. & Aziz, A.A. 2016. Recent advances in synthesis and surface modification of superparamagnetic iron oxide nanoparticles with silica. *Journal of Magnetism and Magnetic Materials* 416: 275-291.

Suryanarayana, C. 2001. Mechanical alloying and milling. *Progress in Material Science* 46(12): 1-184.

Suryanarayana, C., Chen, G.H. & Samfroes, F.H. 1992. Milling maps for phase identification during mechanical alloying. *Scripta Metallurgica et Materialia* 26: 1727-1732.

Tan, P., Sun, J., Hu, Y., Fang, Z., Bi, Q., Chen, Y. & Cheng, J. 2015. Adsorption of Cu^{2+}, Cd^{2+} and Ni^{2+} from aqueous single metal solutions on graphene oxide membranes. *Journal of Hazardous Materials* 297: 251-260.

Nur Asyikin Ahmad Nazri, Ismayadi Ismail & Norlaily Mohd Saiden
Material Synthesis and Characterization Laboratory (MSCL)
Institute of Advanced Technology (ITMA)
Universiti Putra Malaysia
43400 UPM Serdang, Selangor Darul Ehsan
Malaysia

Raba'ah Syahidah Azis*, Muhammad Syazwan Mustaffa, Abdul Halim Shaari & Norlaily Mohd Saiden
Department of Physics
Faculty of Science
Universiti Putra Malaysia
43400 UPM Serdang, Selangor Darul Ehsan
Malaysia

Nur Asyikin Ahmad Nazri
Center of Foundation Studies
Cawangan Selangor
Universiti Teknologi MARA
40450 Shah Alam
Selangor Darul Ehsan
Malaysia

Hasfalina Che Man
Department of Biological and Agricultural Engineering
Faculty of Engineering
Universiti Putra Malaysia
43400 UPM Serdang, Selangor Darul Ehsan
Malaysia

Nor Hapishah Abdullah
Functional Device Laboratory (FDL)
Institute of Advanced Technology (ITMA)
Universiti Putra Malaysia
43400 UPM Serdang, Selangor Darul Ehsan
Malaysia

*Corresponding author; email: rabaah@upm.edu.my